Maciej PAŃCZYK
Jan SIKORA

DECAY FUNCTION INFINITE BOUNDARY ELEMENT APPLICATION IN OPTICAL TOMOGRAPHY

ABSTRACT *Early detection or screening examination of breast cancer can be done using Optical Tomography and Boundary Element Method. We can not make measurements or precisely define boundary conditions on the surface between breast and chest. A few models which uses an extension of the definition area to other tissues surrounding the breast are discussed. Among them model containing infinite boundary elements which allows us to reduce the mesh and to avoid the problem of setting incorrect boundary conditions on unavailable surface between breast and chest.*

Keywords: *Boundary Element Method, Infinite Elements, Optical Tomography*

1. INTRODUCTION

Optical Tomography and Electrical Impedance Tomography can use Boundary Element Method (BEM) for forward problem solution [7]. On the area

Maciej PAŃCZYK, PhD Eng.
e-mail: maciejp@cs.pollub.pl
Wydział Elektrotechniki i Informatyki, Instytut Informatyki, Politechnika Lubelska

Jan SIKORA, PhD DSc Eng.
e-mail: sik59@wp.pl
Wydział Elektrotechniki i Informatyki, Katedra Elektroniki, Politechnika Lubelska
Zakład Metrologii i Badań Nieniszczących, Instytut Elektrotechniki

PROCEEDINGS OF ELECTROTECHNICAL INSTITUTE, Issue 256, 2012

of human female breast cancers investigations it is only possible to make measurements on the skin. The boundary surface between breast and chest remains unavailable for detectors placement. It is also difficult to set precise boundary condition on that surface. A typical simple BEM solution is to extend the boundary element mesh outside the zone of interest and to truncate it at a large distance away so that the new boundary does not influence the results. Such solution generates a large number of additional boundary elements and in case that truncation occurs too near can introduce an unknown error. A more effective method is to incorporate infinite boundary elements [3, 5] into conventional BEM analysis. Infinite elements usage was at first adopted in wave propagation and geotechnical problems [4]. In our case it is to estimate the differences between models and to consider if model with implemented infinite elements offers similar accuracy like these with extended area.

2. THEORY

There are two main lines of infinite elements development: mapped infinite elements where the element is transformed from finite to infinite domain and decay functions infinite elements which uses special decay functions in conjunction with ordinary boundary element interpolation functions [7].

Both types offers similar accuracy. For present investigations decay function infinite elements based on standard eight nodes quadrilateral isoparametsic boundary elements where chosen (Figure 1). Of course final mesh will consists of both ordinary and infinite boundary elements.

The basis interpolation functions N_i (index i corresponds to element nodes $i = 0\ldots7$) for ordinary quadrilateral boundary elements are given by the following formulas (1):

$$
\begin{aligned}
N_0(\xi,\eta) &= -(1-\xi)(1-\eta)(1+\xi+\eta)/4,\\
N_1(\xi,\eta) &= (1-\xi^2)(1-\eta)/2,\\
N_2(\xi,\eta) &= -(1+\xi)(1-\eta)(1-\xi+\eta)/4,\\
N_3(\xi,\eta) &= (1+\xi)(1-\eta^2)/2,\\
N_4(\xi,\eta) &= -(1+\xi)(1+\eta)(1-\xi-\eta)/4,\\
N_5(\xi,\eta) &= (1-\xi^2)(1+\eta)/2,\\
N_6(\xi,\eta) &= -(1-\xi)(1+\eta)(1+\xi-\eta)/4,\\
N_7(\xi,\eta) &= (1-\xi)(1-\eta^2)/2.
\end{aligned}
\tag{1}
$$

The Basic idea of the decay infinite elements is that the ordinary basis interpolation functions N_i (1) are multiplied by a decay functions D_i (3). That combination ensures that the behavior of the element, results that field variable tends to its value at infinity. Basis interpolation functions for the decay infinite elements are then constructed as:

$$M_i(\xi,\eta) = N_i(\xi,\eta) D_i(\xi,\eta). \tag{2}$$

Infinite basis interpolation functions M_i (2) must be unity at its own node. That means that decay functions D_i also have to be equal to one at its own node and tends to far field value at infinity. Transformation of 8 node quadrilateral boundary element into relevant decay infinite element which extends into infinity in one (positive) ξ direction is presented on Figure 1a.

Decay infinite basis interpolation functions can be also developed for both ξ and η directions. Infinite element which extends into infinity in both (positive) ξ and η directions is presented on Figure 1b.

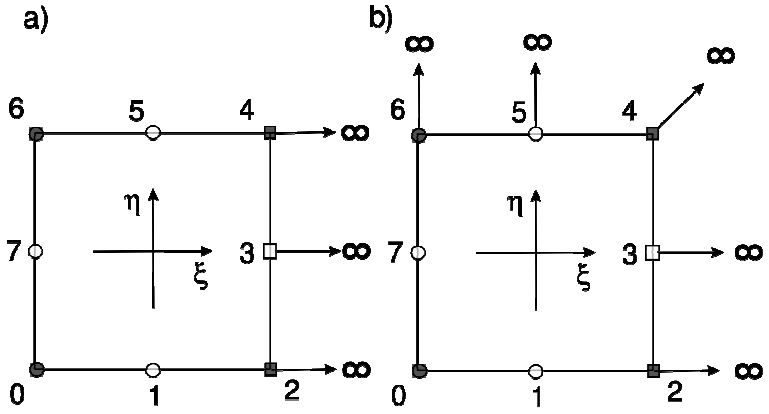

Fig. 1. Transformation of standard 8 node quadrilateral boundary element into decay type infinite element: a) in one ξ direction; b) in two ξ and η directions

Further considerations will be related to reciprocal decay functions of the form:

$$D_i(\xi,\eta) = \left(\frac{\xi_i - \xi_0}{\xi - \xi_0} \right)^n, \tag{3}$$

where: exponent n has to be greater than the highest power of ξ encountered in M. ξ_0 is some origin point located outside the element on the opposite side to that which extends to infinity. Its role is to avoid singularity within the element.

In case of transforming the element into infinity in both directions ξ and η reciprocal decay functions is written as:

$$D_i(\xi,\eta)=\left(\frac{\xi_i-\xi_0}{\xi-\xi_0}\right)^n\left(\frac{\eta_i-\eta_0}{\eta-\eta_0}\right)^m, \tag{4}$$

where: exponent m has to be greater than the highest power of η encountered in M.

For quadratic basis interpolation function, exponent $n = 3$ infinite functions M_i are given by the formulas:

$$\begin{aligned}
M_0(\xi,\eta)&=-(1-\xi)(1-\eta)(1+\xi+\eta)/4\left[(1-\xi_0)/(\xi-\xi_0)\right]^3,\\
M_1(\xi,\eta)&=(1-\xi^2)(1-\eta)/2\left[(-\xi_0)/(\xi-\xi_0)\right]^3,\\
M_2(\xi,\eta)&=-(1+\xi)(1-\eta)(1-\xi+\eta)/4\left[(1-\xi_0)/(\xi-\xi_0)\right]^3,\\
M_3(\xi,\eta)&=(1+\xi)(1-\eta^2)/2\left[(1-\xi_0)/(\xi-\xi_0)\right]^3,\\
M_4(\xi,\eta)&=-(1+\xi)(1+\eta)(1-\xi-\eta)/4\left[(1-\xi_0)/(\xi-\xi_0)\right]^3,\\
M_5(\xi,\eta)&=(1-\xi^2)(1+\eta)/2\left[(-\xi_0)/(\xi-\xi_0)\right]^3,\\
M_6(\xi,\eta)&=-(1-\xi)(1+\eta)(1+\xi-\eta)/4\left[(-1-\xi_0)/(\xi-\xi_0)\right]^3,\\
M_7(\xi,\eta)&=(1-\xi)(1-\eta^2)/2\left[(-1-\xi_0)/(\xi-\xi_0)\right]^3.
\end{aligned} \tag{5}$$

For debugging purposes in case of decay type infinite basis interpolation function the same test as for ordinary basis interpolation functions can be used. It is to check if all basis interpolation functions sum to unity and all the derivatives to zero. The simple test is to check if each function has unit value on their own node and zero on the others. Infinite decay type basis interpolation functions graphs are presented on figure 2.

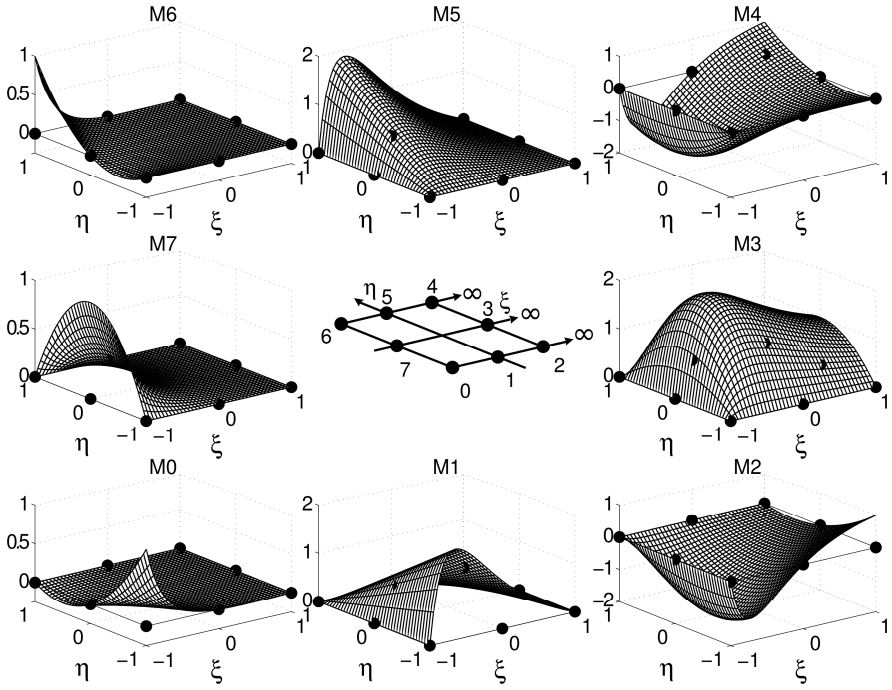

Fig. 2. Basis interpolation functions M0, M1, M2, M3, M4, M5, M6 and M7, eqn. (2), for decay type infinite boundary element

To study boundary elements which are two-dimensional structures placed in the 3D space, first we need to define the way in which we can pass from the x,y,z global Cartesian system to the ξ,η,ζ system defined over the element, where ξ and η are oblique coordinates and ζ is in the direction of the normal. The transformation for a given function Φ is related through the following:

$$\begin{bmatrix} \frac{\partial \Phi}{\partial \xi} \\ \frac{\partial \Phi}{\partial \eta} \\ \frac{\partial \Phi}{\partial \zeta} \end{bmatrix} = \begin{bmatrix} \frac{\partial x}{\partial \xi} & \frac{\partial y}{\partial \xi} & \frac{\partial y}{\partial \xi} \\ \frac{\partial x}{\partial \eta} & \frac{\partial y}{\partial \eta} & \frac{\partial z}{\partial \eta} \\ \frac{\partial x}{\partial \zeta} & \frac{\partial y}{\partial \zeta} & \frac{\partial z}{\partial \zeta} \end{bmatrix} \begin{bmatrix} \frac{\partial \Phi}{\partial x} \\ \frac{\partial \Phi}{\partial y} \\ \frac{\partial \Phi}{\partial z} \end{bmatrix} \tag{6}$$

where the square matrix is the Jacobian matrix (or Jacoby matrix).

Transformation of this type allows us to describe differentials of surface in the Cartesian system in terms of the curvilinear coordinates. A differential of area will be given by:

$$\partial\Gamma = \mathbf{n}\partial\xi\partial\eta = \left|\frac{\partial \mathbf{r}}{\partial \xi} \times \frac{\partial \mathbf{r}}{\partial \eta}\right| \partial\xi\partial\eta = \sqrt{n_x^2 + n_y^2 + n_z^2}\,\partial\xi\partial\eta, \tag{7}$$

where:

$$n_x = \frac{\partial y}{\partial \xi}\frac{\partial z}{\partial \eta} - \frac{\partial y}{\partial \eta}\frac{\partial z}{\partial \xi} \quad ,$$

$$n_y = \frac{\partial x}{\partial \xi}\frac{\partial z}{\partial \eta} - \frac{\partial x}{\partial \eta}\frac{\partial z}{\partial \xi} \quad ,$$

$$n_z = \frac{\partial x}{\partial \xi}\frac{\partial y}{\partial \eta} - \frac{\partial x}{\partial \eta}\frac{\partial y}{\partial \xi}$$

This mapping introduces the Jacobian J proportional to the magnitude of the area of the mapped boundary element. The first derivatives of the mapped interpolation functions with respect to the ξ for infinite element are given by:

$$\frac{\partial M_0(\xi,\eta)}{\partial \xi} = -\frac{(\xi_0+1)^3(\eta-1)\left(2\xi\eta+\xi_0\eta-3\eta+\xi^2+2\xi_0\xi-3\right)}{4(\xi-\xi_0)^4},$$
$$\frac{\partial M_1(\xi,\eta)}{\partial \xi} = \frac{\xi_0^3(\eta-1)\left(\xi^2+2\xi_0\xi-3\right)}{2(\xi-\xi_0)^4},$$
$$\frac{\partial M_2(\xi,\eta)}{\partial \xi} = -\frac{(\xi_0-1)^3(\eta-1)\left(-2\xi\eta-\xi_0\eta-3\eta+\xi^2+2\xi_0\xi-3\right)}{4(\xi-\xi_0)^4},$$
$$\frac{\partial M_3(\xi,\eta)}{\partial \xi} = -\frac{(\xi_0-1)^3\left(\eta^2-1\right)(2\xi+\xi_0+3)}{2(\xi-\xi_0)^4},$$
$$\frac{\partial M_4(\xi,\eta)}{\partial \xi} = \frac{(\xi_0-1)^3(\eta+1)\left(2\xi\eta+\xi_0\eta+3\eta+\xi^2+2\xi_0\xi-3\right)}{4(\xi-\xi_0)^4},$$
$$\frac{\partial M_5(\xi,\eta)}{\partial \xi} = -\frac{\xi_0^3(\eta+1)\left(\xi^2+2\xi_0\xi-3\right)}{2(\xi-\xi_0)^4},$$
$$\frac{\partial M_6(\xi,\eta)}{\partial \xi} = \frac{(\xi_0+1)^3(\eta+1)\left(-2\xi\eta-\xi_0\eta+3\eta+\xi^2+2\xi_0\xi-3\right)}{4(\xi-\xi_0)^4},$$
$$\frac{\partial M_7(\xi,\eta)}{\partial \xi} = \frac{(\xi_0+1)^3\left(\eta^2-1\right)(2\xi+\xi_0-3)}{2(\xi-\xi_0)^4}, \tag{8}$$

$$\frac{\partial M_0(\xi,\eta)}{\partial \eta} = \frac{(\xi_0+1)^3(\xi-1)(2\eta+\xi)}{4(\xi-\xi_0)^3},$$
$$\frac{\partial M_1(\xi,\eta)}{\partial \eta} = -\frac{\xi_0^3\left(\xi^2-1\right)}{2(\xi-\xi_0)^3},$$
$$\frac{\partial M_2(\xi,\eta)}{\partial \eta} = \frac{(\xi_0-1)^3(\xi+1)(\xi-2\eta)}{4(\xi-\xi_0)^3},$$
$$\frac{\partial M_3(\xi,\eta)}{\partial \eta} = \frac{(\xi_0-1)^3(\xi+1)\eta}{(\xi-\xi_0)^3},$$
$$\frac{\partial M_4(\xi,\eta)}{\partial \eta} = -\frac{(\xi_0-1)^3(\xi+1)(2\eta+\xi)}{4(\xi-\xi_0)^3},$$
$$\frac{\partial M_5(\xi,\eta)}{\partial \eta} = \frac{\xi_0^3\left(\xi^2-1\right)}{2(\xi-\xi_0)^3},$$
$$\frac{\partial M_6(\xi,\eta)}{\partial \eta} = -\frac{(\xi_0+1)^3(\xi-1)(\xi-2\eta)}{4(\xi-\xi_0)^3},$$
$$\frac{\partial M_7(\xi,\eta)}{\partial \eta} = \frac{(\xi_0+1)^3(1-\xi)\eta}{(\xi-\xi_0)^3}. \tag{9}$$

The boundary integral equation containing both finite (surface covered by ordinary boundary elements) and infinite boundary elements (surface covered by infinite decay function boundary elements) after discretization will take the form:

$$
\begin{aligned}
&c(\mathbf{r})\Phi_i(\mathbf{r}) + \sum_{i=0}^{std-1}\sum_{k=0}^{7}\int_{-1}^{+1}\int_{-1}^{+1}\Phi(\mathbf{r}')N_k(\xi,\eta)\frac{\partial G\left(|\mathbf{r}-\mathbf{r}'|\right)}{\partial n}J^N(\xi,\eta)\partial\xi\partial\eta + \\
&+\sum_{i=0}^{\inf-1}\sum_{k=0}^{7}\int_{-1}^{+1}\int_{-1}^{\infty}\Phi(\mathbf{r}')M_k(\xi,\eta)\frac{\partial G\left(|\mathbf{r}-\mathbf{r}'|\right)}{\partial n}J^M(\xi,\eta)\partial\xi\partial\eta = \\
&=\sum_{i=0}^{std-1}\sum_{k=0}^{7}\int_{-1}^{+1}\int_{-1}^{+1}\frac{\partial\Phi(\mathbf{r}')}{\partial n}N_k(\xi,\eta)G\left(|\mathbf{r}-\mathbf{r}'|\right)J^N(\xi,\eta)\partial\xi\partial\eta + \\
&+\sum_{i=0}^{\inf-1}\sum_{k=0}^{7}\int_{-1}^{+1}\int_{-1}^{\infty}\frac{\partial\Phi(\mathbf{r}')}{\partial n}M_k(\xi,\eta)G\left(|\mathbf{r}-\mathbf{r}'|\right)J^M(\xi,\eta)\partial\xi\partial\eta
\end{aligned}
\tag{10}
$$

For singularity treatment as one of the most effective, regularization method [7] was used. The advantage of using that method is that the calculation schema remains unchanged for infinite elements.

3. MODELS

Four simple theoretical models of human breast were investigated. For all models one placement of the light source was presented – located near the bottom of the hemisphere model. First model presented on Figure 3 corresponds to the pure hemisphere. Second model was extended by adding a cylinder in the bottom (Fig. 4). The intention of it was to avoid possible errors on the bottom of the hemisphere. The next one develop that idea by adding the cylinder with identical height but bigger diameter (Fig. 5). It is to eliminate the errors near the basis circumference. All models were constructed from 1536 second order eight nodes quadrilateral boundary elements and 4610 nodes. Half of the elements covers hemisphere.

Governing equation for the problem is diffusion approximation of the transport equation [7] (Helmholtz – assuming scattering and absorption are homogeneous):

$$
\nabla^2\Phi(\mathbf{r},\omega) - k^2\Phi(\mathbf{r},\omega) = -\frac{q_0(\mathbf{r},\omega)}{D}, \quad \forall\mathbf{r}\in\Omega/\Gamma, \tag{11}
$$

where Φ stands for photon density, $k = \sqrt{\frac{\mu_a}{D} - j\frac{\omega}{cD}}$ complex wave number, $D = [3(\mu_a + \mu_S')]^{-1}[mm^{-1}]$ diffusion coefficient, μ_S' is reduced scattering coefficient, μ_a is an absorbing coefficient, c speed of light in the medium, q_0 is a source of light (number of photons per volume unit emitted by concentrated light source located in position r with modulation frequency ω).

Generally in Diffusive Optical Tomography distribution of μ_a and μ_s' are investigated.

There are Robin boundary conditions on surfaces [2, 8, 10]:

$$\Phi(\mathbf{r},\omega) + 2\alpha D\frac{\partial\Phi(\mathbf{r},\omega)}{\partial n} = 0, \quad \forall \mathbf{r} \in \Gamma. \tag{12}$$

with different coefficients for breast tissue and for skeletal muscles on the basis [2, 8, 10] imposed. In analysed example the following breast tissue properties were taken [2, 10]: $\mu_a = 0.025[mm^{-1}], \mu_s' = 2[mm^{-1}], \alpha = 1, f = 100MHz$.

Last open boundary model consists from 768 standard boundary elements and 64 infinite decay type elements based on eight nodes second order quadrilateral boundary elements [5, 9]. The number of nodes is reduced to 2561 nodes in that case (Fig. 6).

Decay function infinite basis approximation functions [5] were used for element transformation like presented on Figure 1. Relevant boundary integral equation for surfaces covered by standard and infinite elements can be written as:

$$\begin{aligned} &C(\mathbf{r})\Phi(\mathbf{r}) + \int_{\Omega}\frac{\partial G(|\mathbf{r}-\mathbf{r}'|,\omega)}{\partial n}\Phi(\mathbf{r}')d\Omega + \\ &+ \int_{\Omega_\infty}\frac{\partial G(|\mathbf{r}-\mathbf{r}'|,\omega)}{\partial n}\Phi(\mathbf{r}')d\Omega_\infty = \int_{\Omega} G(|\mathbf{r}-\mathbf{r}'|,\omega)\frac{\partial\Phi(\mathbf{r}')}{\partial n}d\Omega + \\ &+ \int_{\Omega_\infty} G(|\mathbf{r}-\mathbf{r}'|,\omega)\frac{\partial\Phi(\mathbf{r}')}{\partial n}d\Omega_\infty - \sum_{S=0}^{n_S-1} Q_S G(|\mathbf{r_S}-\mathbf{r}|,\omega) \end{aligned} \tag{13}$$

where Q_S is the magnitude of the concentrated source ($q_0 = Q_S\delta(r_S)$) and n_S is a number of these sources, Φ stands for the photon density and G is the fundamental solution for the diffusion equation [2, 8, 10]. In 3D space for the diffusion equation the fundamental solution is [7]:

$$G(|\mathbf{r}-\mathbf{r}'|,\omega) = \frac{1}{4\pi|\mathbf{r}-\mathbf{r}'|}e^{-k|\mathbf{r}-\mathbf{r}'|}. \tag{14}$$

The normal derivative of the Green function in a direction n can be written:

$$\mathbf{n}\cdot\nabla G = \mathbf{n}\cdot\frac{\mathbf{r}-\mathbf{r}'}{|\mathbf{r}-\mathbf{r}'|}\left(\frac{-1}{4\pi|\mathbf{r}-\mathbf{r}'|^2}-\frac{k}{4\pi|\mathbf{r}-\mathbf{r}'|}\right)e^{-k|\mathbf{r}-\mathbf{r}'|}. \tag{15}$$

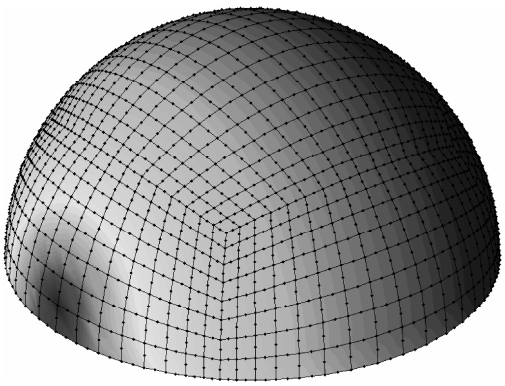

Fig. 3. Base model of the breast – hemisphere

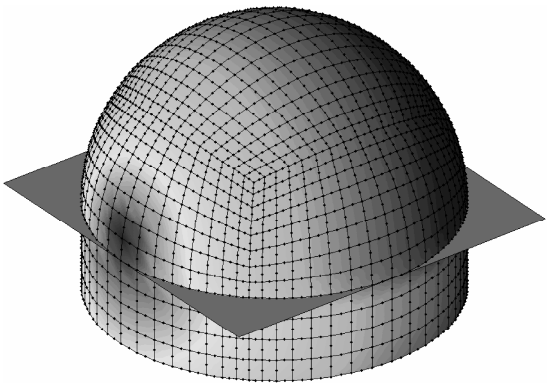

Fig. 4. Extended model with additional part of chest, hemisphere with cylinder on the bottom

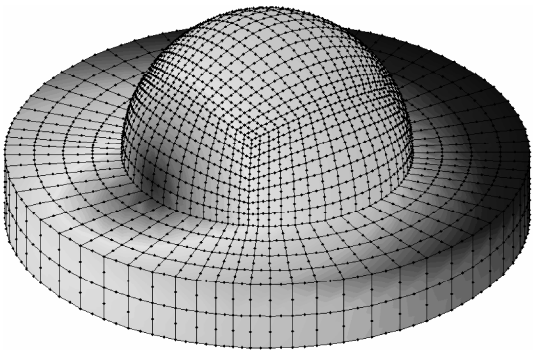

Fig. 5. Extended model with additional part of chest, hemisphere with wider cylinder on the bottom

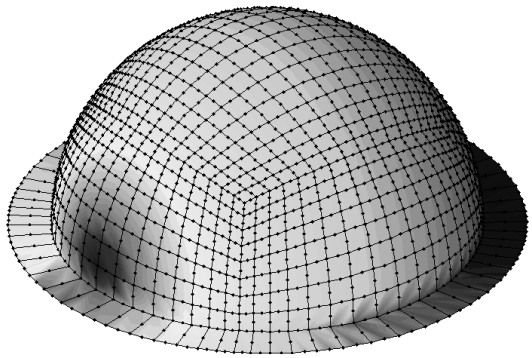

Fig. 6. Open boundary hemisphere breast model with infinite boundary elements on the bottom

4. RESULTS

Values of $\partial\Phi/\partial$n module and phase of the light at hemisphere circumference cross-section for $y = 0$ are presented on Figure 7 and 8 respectively. To estimate the solution differences models with extended bottom part – Figure 4, 5 and 6 were compared to basic hemisphere one – Figure 3. Generally three

extended models offers similar results, remarkably different then achieved while using the simplest hemisphere one. It is to notice that there is a logarithmic scale on $\partial\Phi/\partial n$ module graph 7. The medium approximation differences for module reaches 50% and for phase oscillates mainly about 3%.

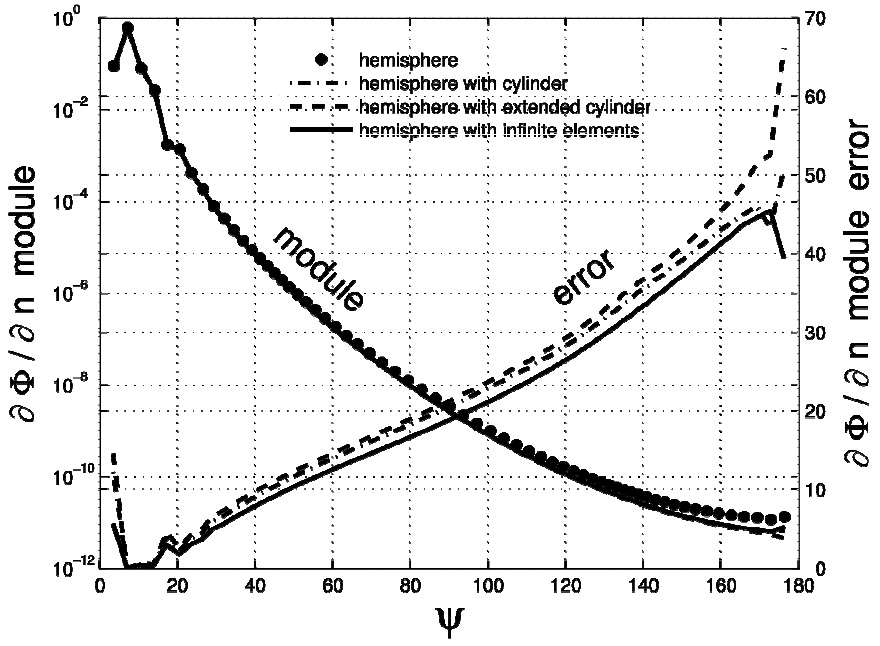

Fig. 7. Results comparison for $\partial\Phi/\partial n(\Psi)$ module and solution differences compared to hemisphere model

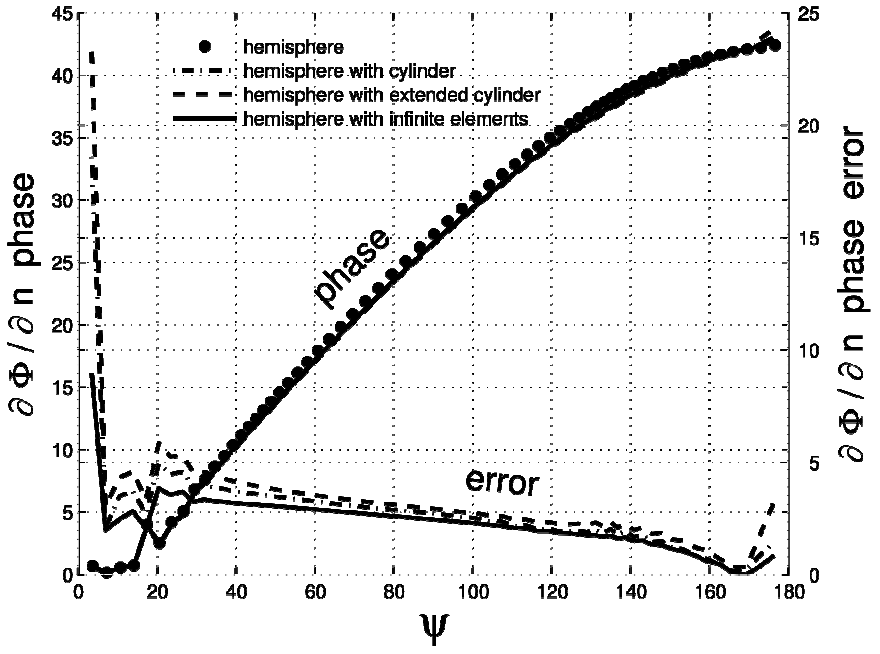

Fig. 8. Results comparison for $\partial\Phi/\partial n(\Psi)$ phase and solution differences compared to hemisphere model

5. CONCLUSION

Generally three extended breast models (these with added additional cylindrical part on the hemisphere basis or with infinite elements incorporated) offers similar accuracy – Figures 7 and 8. Significantly worst results were achieved from the pure hemisphere model. Medium differences between hemisphere and extended models for module reaches 50% and for phase about 3%. Fifty percent differences are enough significant to extend the mesh and to include in calculations not only the breast tissue represented by hemisphere but also a part of chest with muscles and bones relevant to additional cylindrical part or ring consisting of infinite elements. The advantage of using infinite elements is to shorten the calculation time and keep the accuracy similar to extended models. Reducing the number of mesh elements almost to 50% is fundamental for inverse problem solution when the forward problem has to be calculated many times. All extended models were built from the same number of standard 8-node second order quadrilateral boundary elements. Mesh density on the additional surface related to cylindrical part of the model was lower then on the hemisphere surface. This is typical practical solution, as the additional part represents the region outside the zone of interests, and is included only to improve the accuracy. Except models mentioned above which consists of 1536 elements and 4610 nodes, calculations were done also for models covered by 384 elements and 1154 nodes as well as 6144 elements and 18434 nodes. Results calculated from the simplest model build from 384 elements had little oscillations instead of smooth solution. Model with the highest mesh density, 6144 elements, required too much memory and took too long calculation time without significant accuracy improvement. Calculations takes 18 seconds for 384 node models and 4 minutes and 47 seconds in case of 4160 node models. Model with infinite elements build from 832 elements which is relevant to standard one build from 1536 elements and 4610 nodes required 1 minute and 24 seconds for calculations. Self made generator was used to build presented meshes containing only quadrilateral elements and to create open boundary models with infinite boundary elements. Application of infinite boundary elements into Boundary Element Method approves computational efficiency comparing to mesh truncation. The process of incorporating infinite elements into BEM calculation scheme is quite logical. Presented application in Optical or Electrical Impedance mammography can be used as a screening examination in breast cancer detection but infinite elements can be used also for other purposes.

REFERENCES

1. Abramowitz I.A.: Stegun. Handbook of mathematical functions with formulas, graphs and mathematical tables. John Wiley, New York, 1973.
2. Arridge S.R.: Optical tomography in medical imaging, Inverse Problems, vol. 15, No. 2 (1999), pp. R41-R93.
3. Beer G., Watson J.O.: Infinite Boundary Elements, International Journal for Numerical Methods in Engineering, vol. 28 (1989), pp. 1233-1247.
4. Beer G., Watson J.O., Swoboda G.: Three-dimensional analysis of tunnels using infinite boundary elements, Computers and Geotechnics, vol. 3 (1987), pp. 37-58.
5. Bettess P.: Infinite Elements, Penshaw Press, 1992.
6. Gratkowski S.: Asymptotyczne warunki brzegowe dla stacjonarnych zagadnień elektromagnetycznych w obszarach nieorganicznych – algorytmy metody elementów skończonych, Wydawnictwo Uczelniane Zachodniopomorskiego Uniwersytetu Technologicznego w Szczecinie, 2009.
7. Sikora J.: Boundary Element Method for Impedance and Optical Tomography, Oficyna Wydawnicza Politechniki Warszawskiej, Warsaw, 2007.
8. Tarvainen T.: Computational Methods for Light Transport in Optical Tomography, PhD Thesis, Department of Physics, University of Kuopio, (2006), http://physics.uku.fi/vilhunen/phdthesis_ttarvainen.pdf
9. Watson J.O.: Advanced implementation of the boundary element method for two- and three-dimensional elastostatics, Developments in Boundary Element Methods – 1 (Editors P.K. Banerjee and R. Butterfield), Elsevier Applied Science Publishers, vol. 61 (1979), pp. 31-63.
10. Zacharopoulos A., Arridge S.R., Dorn O., Kolehmainen V., Sikora J.: Three-dimensional reconstruction of shape and piecewise constant region values for optical tomography using spherical harmonic parametrization and a boundary element method, Inverse Problems, vol. 22 (2006), pp. 1-24.

Manuscript submitted 16.04.2012 r.

ZASTOSOWANIE ELEMENTÓW BRZEGOWYCH NIESKOŃCZONYCH Z FUNKCJAMI ZANIKU W TOMOGRAFII OPTYCZNEJ

Maciej PAŃCZYK, Jan SIKORA

STRESZCZENIE *Wczesne przesiewowe wykrywanie nowotworów piersi może być wykonywane z zastosowaniem Metody Elementów Brzegowych i mammografii optycznej. Wymaga to określenia warunków brzegowych. Niestety, nie ma możliwości umieszczenia*

detektorów i źródeł światła na powierzchni między piersią a klatką piersiową. Typowym rozwiązaniem jest rozszerzenie obszaru poszukiwania rozwiązania o fragment klatki piersiowej i utworzenie sztucznej granicy zaniku zjawiska. Zbytnie powiększenie siatki skutkuje wzrostem kosztów obliczeniowych, natomiast przyjęcie sztucznej granicy zbyt blisko obszaru zainteresowań – powstaniem potencjalnych błędów. Rozważania przeprowadzono na bazie kilku prostych modeli piersi. Ostatni model zawiera elementy brzegowe nieskończone pozwalające na zredukowanie rozmiarów siatki i uniknięcie problemu błędnych warunków brzegowych przez utworzenie modelu o tzw. otwartym brzegu

Słowa kluczowe: *Metoda elementów brzegowych, elementy nieskończone, tomografia optyczna*

Maciej PAŃCZYK, PhD Eng. – graduated from the Faculty of Electrical Engineering, Lublin University of Technology. He worked in the Department of Fundamental Electrical Engineering, Lublin University of Technology, then in Information Technology Departament in Bank BDK S.A and since 2004 at the Institute of Computer Science, Lublin University of Technology. His work focuses on the electromagnetic field and programming.

Prof. Jan SIKORA, PhD. DSc. Eng. – graduated from Warsaw University of Technology Faculty of Electrical Engineering. During over 34 years of professional work he has proceeded all grades, titles and positions including the position of full professor at his alma mater. He worked for the Institute of Electrical Engineering in Warsaw since 1998. Since 2008 he worked at Electrical Engineering and Computer Science Faculty In Lublin University of Technology in the Department of Electronics. In 2001-2004 he worked as a Senior Research Fellow at University College London in the prof. S. Arridge's Group of Optical Tomography. His research interests are focused on numerical methods for electromagnetic field.